Submitted to the 29th International Conference on High-Energy Physics ICHEP98,
Vancouver, Canada, July 1998

Fragmentation Measurements in the Breit Frame at HERA

H1 Collaboration

Abstract

Deep inelastic positron-proton scattering data, taken in 1996 at the H1 detector at HERA, are analysed in the Breit frame of reference. Violations of scale invariance in the current hemisphere fragmentation functions for charged particles are compared with a NLO QCD expectation. The evolution of the peak and width of the fragmentation function, and the average charged multiplicity are presented as a function of the photon virtuality, Q. Rapidity distributions are shown at low and high Q, and as a function of transverse momentum. Comparisons are made with particle production in e^+e^- annihilation at equivalent centre of mass energies, with MLLA calculations, and with current perturbative QCD Monte Carlo models.

Abstract: 531
Parallel sessions: 3,5
Plenary sessions: 5,7

1 Introduction

In previous publications [1, 2, 3] HERA experiments analysed hadron production in ep deep–inelastic scattering in the Breit frame of reference. Similarities were demonstrated between hadronic distributions in the 'current' hemisphere of this frame of reference and those in a single hemisphere of an e^+e^- annihilation interaction, with significant differences being attributable to leading order processes which occur in DIS but not in e^+e^- interactions. Note that ep experiments are able to measure the energy evolution of such distributions in a single experiment, considerably reducing point–to–point systematic errors.

The present paper uses data samples from the H1 experiment taken in 1996. Compared to the last publication [2] the data are of higher quality and are quantitatively more than factors of four (or six) times greater at low (or high) Q^2. This analysis extends both the kinematic range and the range of physical variables measured.

After a description of the relevant parts of the apparatus (section 2) and a discussion of the treatment of the data (section 3), we describe the Breit frame of reference (section 4) and then study scaling violations (section 5), the evolution of the fragmentation function (section 6), invariant spectra (section 7) and rapidity distributions (section 8).

2 The H1 Detector

The H1 detector is described in detail elsewhere [6]. Here, we give only a short description of the components more relevant to this analysis. We employ a right-handed coordinate system with the positive (forward) z axis being in the direction of the incoming proton beam. Polar angles are measured from this direction.

Momentum measurements of charged particles are provided, in the central region of the apparatus, by two cylindrical and co-axial drift chambers [7] for (r, ϕ) measurement, supplemented by two z-chambers. In the forward (proton) direction the equivalent measurements are provided by the Forward Track Detector (FTD [8]) which consists of three Radial and three Planar drift chamber modules. All these track detectors are inside a uniform 1.15 T magnetic field. Track segments from all devices are combined to give efficient detection and momentum measurement with $\delta p/p^2 \lesssim 1\%$ /GeV for most of the angular range used in this analysis, $10° < \theta < 160°$.

In the polar angle range $4° < \theta < 154°$ the trackers are surrounded by a fine-grained liquid argon (LAr) sampling calorimeter [9] with lead and steel absorber in the electromagnetic and hadronic sections respectively. This calorimeter also triggers on, and measures, the energy of the scattered positron for high Q^2 events (selected to be $Q^2 \geq 100$ GeV^2). A backward scintillating fibre calorimeter (SPACAL [10]) covers the range $153° < \theta < 177.8°$ and provides the trigger and measurement of the positron in the sample referred to as low Q^2 events (selected to be $Q^2 \geq 12$ GeV^2). The SPACAL detector also gives time of flight information for the efficient removal of beam related background.

3 Data Selection and Corrections

The data are taken with 27.5 GeV positrons incident on 820 GeV protons giving an ep centre of mass energy, $\sqrt{s}$, of 300 GeV. The trigger is already fully efficient at positron energies $\sim$ 10 GeV, well below those implied by the kinematic selections made. The analysis begins with nearly two million events of which nearly half a million survive basic fiducial cuts. This corresponds to an integrated luminosity of about 7 pb^{-1}. Event kinematic variables used in this analysis are calculated using only the scattered lepton, which gives both good resolution in the chosen region and explicit freedom from bias on the hadronic system studied. Further cuts are made to ensure energy containment of the scattered positron. These effectively separate the data into the low and high Q^2 samples as mentioned in the previous section.

At low Q^2, the events are explicitly selected to have an identified scattered positron with an energy $E'_e > 14$ GeV and with kinematic quantities which would imply that a massless quark would be scattered through $10° < \theta < 150°$. This is inside the acceptance of the H1 track detectors and thus minimises corrections, at the cost of removing a further $\sim 24\%$ of events.

To reject beam associated background, we demand that there be no veto from the time of flight system and that, in the z coordinate, a vertex be found for the event within 35 cm of the nominal vertex position. The dimensionless inelasticity variable, $y = Q^2/xs$, is required to be in the range $0.05 < y < 0.6$, and the sum $\Sigma_i(E^i - p_z^i)$ over all calorimeter energy deposits is required to be larger than 35 GeV. Together, these conditions ensure that contamination from mis-identified photoproduction events is below the 1% level and reduce corrections for QED radiative effects.

An additional cut is placed to safely exclude a further $\sim 6\%$ (1%) of diffractive events at low (high) Q^2 which are not well-modelled with the DIS Monte Carlo programs used in this analysis and which have no analogue in e^+e^- interactions. We require that a total cluster energy of at least 0.5 GeV should be observed in the region $4.4° < \theta < 15°$.

There is a remaining source of error arising from QED radiation which comes about because of an incorrect value of Q^2. The error in the boost leads to a miscalculation of the direction of the Breit frame axis. In most cases, this leads to a depleted or even empty, region of phase space where the scattered quark fragments are expected. With improved statistics this has become a significant effect. To reduce the size of the necessary QED corrections, this analysis reimposes the $0.05 < y < 0.6$ selection using hadronic system variables calculated with the Jaquet Blondel method [11].

Following all of the selection procedures there are 89 734 events at low Q^2 and 7 631 events at high Q^2.

In addition to these *event* selections there are also cuts made to reject badly measured tracks. Any tracks in the central chambers with transverse momentum below 150 MeV and those in the forward track detectors with momentum below 500 MeV are removed. We also remove tracks failing minimum requirements on the number of hits in a given chamber and the quality of the track fit. In order to have only the primary multiplicity, cuts are also made to exclude tracks not originating from the interaction vertex. There remains a small excess contribution due to the decays of short-lived strange particles.

To correct for this excess and for acceptance losses, we utilise the DJANGO6 [12]

Monte Carlo event generator. This combines a leading order (LO) perturbative QCD matrix element calculation and the colour dipole model with a calculation of QED radiative effects. Radiative effects remaining after our event selections have been corrected by comparing the results of Monte Carlo calculations with and without the inclusion of QED radiative effects. The detector response is simulated using a program based on the GEANT [13] package and the simulated events are reconstructed and selected using exactly the same analysis chain as with real data. No particle identification is used in this analysis. We adopt the procedure throughout of assuming that each charged particle is a pion and then using the same Monte Carlo simulation procedure to correct for the $\sim 15\%$ kaon and proton content. The total bin-by-bin corrections made throughout this analysis are generally well within $\pm 20\%$ and vary smoothly in any given distribution.

A large source of systematic error for this analysis originates in possible calibration errors of $\pm 1\%$ for the SPACAL and $\pm 3\%$ for the LAr electromagnetic calorimeter energy scales since they directly affect the accuracy of Lorentz boosts and translate into uncertainties on the number of tracks in the area of interest $\sim \pm 9\%$ throughout, in a highly correlated fashion. The systematic error in the Monte Carlo derived acceptance correction functions has been estimated using two different generators [12, 14] and is $\sim \pm 3\%$.

The full experimental details of how the corrected distributions of this analysis are obtained from the data may be found for example in reference [15].

4 The Breit Frame of Reference

The ep Breit frame is aligned with the hadronic centre of mass (HCM) but boosted along a common z direction such that the incident virtual photon has zero energy, zero transverse momentum and a z component of momentum $-Q$. Both of these frames of reference have the advantage for QCD studies, that transverse momenta associated with the purely electroweak recoil against the scattered electron are removed. In the laboratory frame low p_t tracks are removed (see section 3). Although there is a strong correlation of transverse momentum between the laboratory and Breit frames, the event-to-event variable boosts give sufficient acceptance for the study of low transverse momenta in the Breit frame.

As with the laboratory frame of reference, the Breit frame positive z axis is chosen to be in the direction of the incoming proton and we refer to this as the 'target' hemisphere. The negative z, or photon, direction is referred to as the 'current' hemisphere of the interaction. In the naïve quark parton model (QPM) the massless incoming quark has energy $Q/2$ and z component of momentum $+Q/2$, carrying an approximate fraction x of the proton's momentum. After scattering, it still has energy $Q/2$, with momentum $-Q/2$.

There is excellent acceptance for the current hemisphere in the central H1 detector. Even in the highest Q^2 interval of this analysis there is only a $\sim$8% contribution of uniquely forward (FTD) tracks. Measurements in the target hemisphere, of course, rely heavily on this detector.

When QCD corrections to the parton model are considered, the incident parton carries, in general, a proportion of the incident proton's momentum that is larger than x and has an energy larger than $Q/2$. Furthermore, since the four-momentum of the photon is fixed the energy seen in the current hemisphere may be either greater than or less than $Q/2$. Note that, to order α_s, i.e. two exiting partons as well as the spectator system, DIS events may have *no* energy in the current hemisphere when the incident parton has energy above Q, other than that due to hadronisation [5].

5 Fragmentation Function Scaling Violations

The *ep* Breit frame equivalent of the e^+e^- scaled hadron momentum $x_p = 2p_{hadron}/E^*$ is $x_p = 2p_{hadron}/Q$, where only hadrons in the current hemisphere are considered. The event normalised distribution $D(x_p, Q^2) = (1/N) \times \mathrm{d}n^{\pm}_{tracks}/\mathrm{d}x_p$, the fragmentation function, characterises the processes by which partons shower and then hadronise.

At high enough energies, fragmentation functions approximately scale and are "soft", rising rapidly at small x_p and peaking near $x_p = 0$. As the energy of the initial parton increases, $D(x_p, Q^2)$ follows a QCD evolution into an even softer function with increased probability for low x_p hadrons at the expense of high x_p. In the language of perturbative QCD these scaling violations are caused by time-like partonic showers, directly analogous to the space-like showers which result in energy dependent violations of scaling of the structure function $F_2(x, Q^2)$ [16].

This scaling violation can be seen clearly in Fig. 1 where the fragmentation function is plotted as a function of Q for different intervals of x_p. Typically, in this analysis, the intervals of x_p are much greater than the resolution ($\sim$ 0.01 rms). The resulting purity for each analysis bin (percentage of tracks generated in a given interval which are reconstructed in the same interval) is typically in the range 60-80%. In the same figure, an analysis [3] by the ZEUS collaboration and a prediction from a next-to-leading order (NLO) QCD [17] calculation are compared to the H1 data.

The NLO prediction is shown for the expected infra-red safe range $x_p >\sim 1.54 \times 2m_t/Q$, with the transverse mass, m_t set at 500 MeV. The huge violations at low x_p cannot be described by this approach and are analysed in the next section. At large x_p and large Q^2 there is good agreement of the NLO prediction with data. Theoretical uncertainties in the parameterisations of the fragmentation following the NLO matrix element calculations are presently limiting progress in determining α_s from *ep* fragmentation data.

6 Evolution of the Fragmentation Function

The small x_p region is better investigated using the variable $\xi = \ln(1/x_p)$. According to the expectations of the Modified Leading Logarithmic Approximation (MLLA) and Local Parton Hadron Duality (LPHD), $D(\xi)$ is Gaussian in the neighbourhood of the peak [18].

The increased statistics of this, compared with our earlier, analyses still demonstrates no significant deviation from a Gaussian-like behaviour in the central region. For comparison, Fig. 2 displays two H1 data sets at Q values either side of the E^* value of a TASSO [19] data set, normalised to the same average area.

The evolution of the fragmentation function may be summarised by the Q, or E^*, dependence of the peak and width (dispersion) values of a fitted Gaussian as is shown in Fig. 3. The systematic effects discussed in section 3 contribute only a total $\sim$2.5%

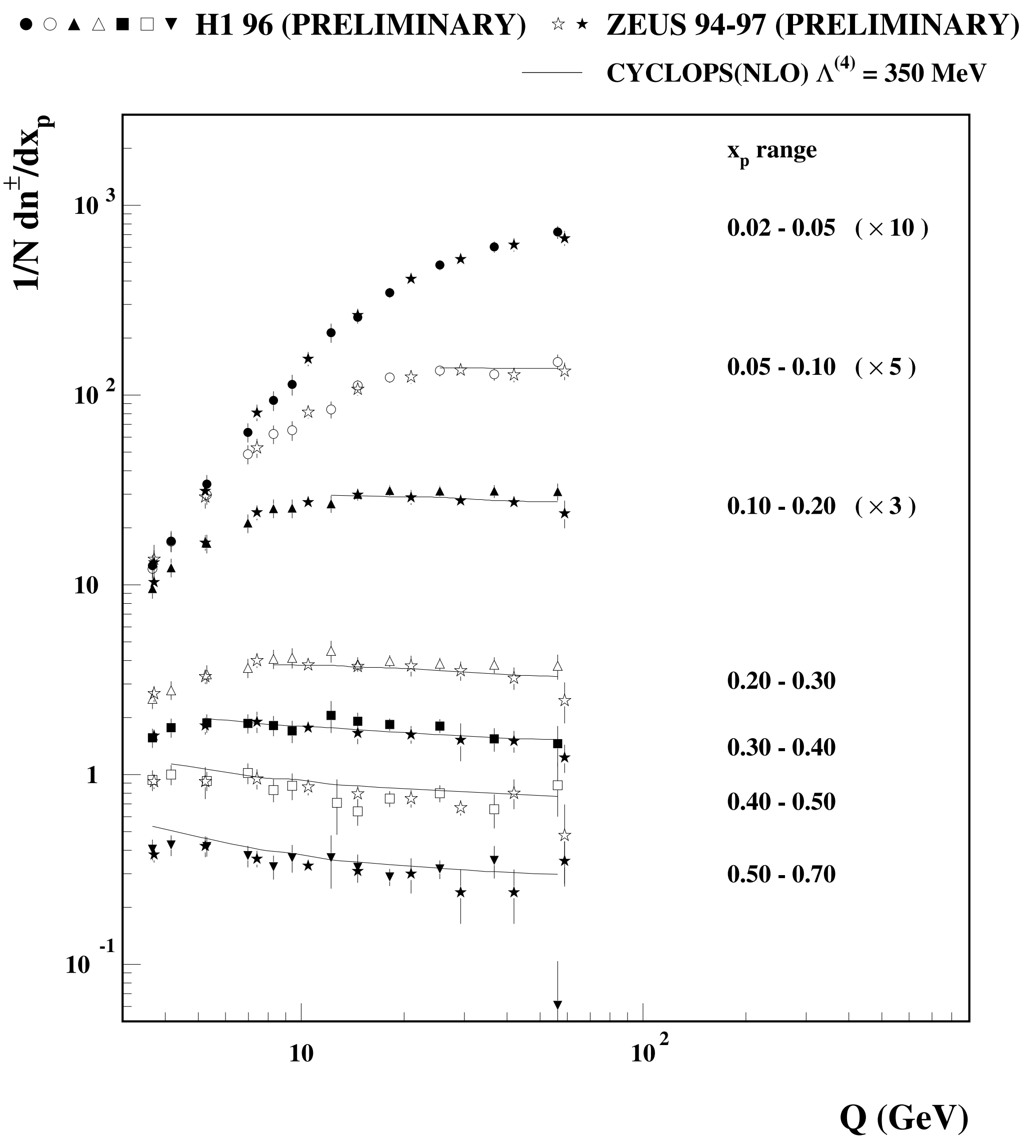

Figure 1: *Scaling violations of the fragmentation function as a function of Q for H1 results and for those from the ZEUS Collaboration (starred symbols) each within the same indicated intervals of the scaled momentum, x_p. Note that the data for the three lowest intervals of x_p are multiplied by factors of 10, 5 and 3 respectively for clarity. Statistical and systematic errors are added in quadrature. The solid lines show the prediction of the CYCLOPS NLO calculation.*

uncertainty to the peak and width measurements. The results are compatible with those published earlier [2], which had considerably lower precision. The results are also broadly compatible with various e^+e^- experiments [19, 20, 21, 22, 23], where the relevant evolution variable is the centre of mass energy, E^*. For this comparison the published e^+e^- data

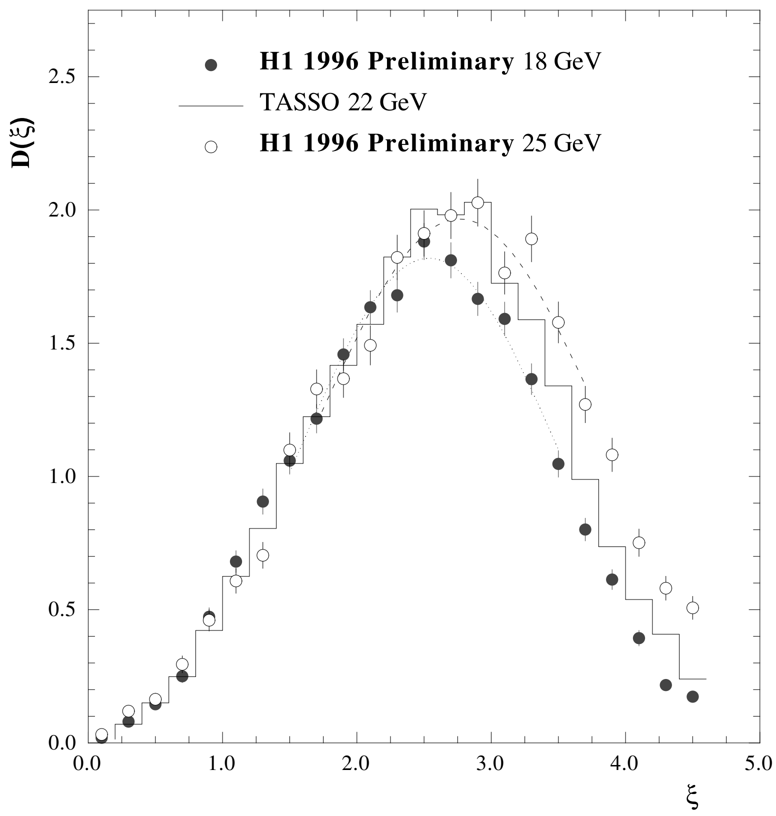

Figure 2: *H1 results for $D(\xi)$ at 18 and 25 GeV in Q compared to TASSO data at 22 GeV in E^*. Statistical and systematic errors are combined in quadrature. The broken lines show the results of Gaussian fits to the H1 data in the range $\pm$ one unit of ξ either side of the mean.*

have been re-fitted to a Gaussian shape in the range $\pm$ one unit of ξ either side of the mean in order to be presented in a directly comparable form.

The results of a simultaneous two–parameter fit of H1 data to MLLA/LPHD expectations incorporating gluon coherence [18] are also shown in Fig. 3(a,b).

The area underneath the fragmentation function is the average charged multiplicity and this is shown, together with results [3] from the ZEUS collaboration, as a function of Q in Fig. 4. We have no experimental evidence for an increase of $\langle n \rangle$ with x at fixed Q. The ep data are compared with a curve which accurately parameterises [24] the average charged multiplicity from many e^+e^- experiments as a function of E^*. The error associated with this fit at any given energy is at the percent level.

Most published e^+e^- results refer to full event multiplicities. Here, as elsewhere in this analysis, track multiplicity data from e^+e^- experiments have been halved to correspond to the fragmentation of one quark. We also reduce published total multiplicity results by a further 8% to account for K^0 and Λ decay tracks [24, 25], and by a variable factor, always below 3%, to correct for the increased multiplicity from b quark fragmentation [26] in e^+e^- .

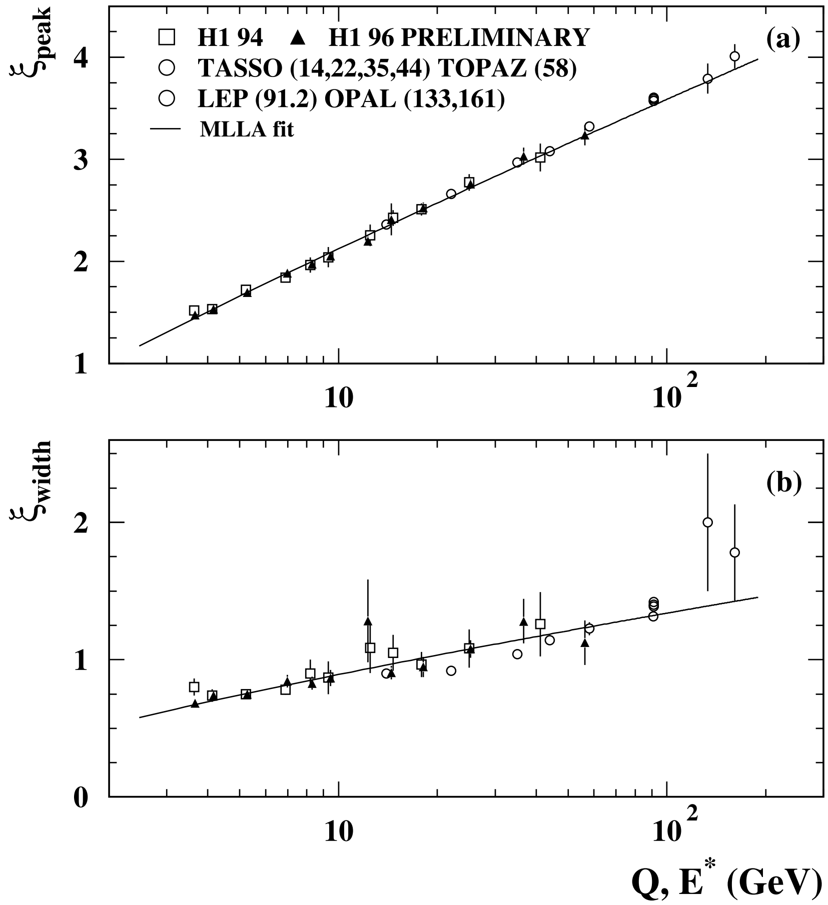

Figure 3: *H1 results (solid symbols, with statistical and systematic errors combined in quadrature) showing the evolution of (a) the peak and (b) the width of the fragmentation function as a function of* Q *compared with* e^+e^- *results (open symbols) as a function of the centre of mass energy,* E^**. The solid line is a fit of H1 data alone to MLLA/LPHD expectations.*

Our earlier analyses [2] established qualitatively that the smaller $\langle n \rangle$ values from *ep* DIS experiments at low Q as compared with e^+e^- annihilation experiments at low E^* could be explained by LO QCD processes, present in *ep* but not in e^+e^- interactions, producing a depletion of the current region of the Breit frame. Pure QPM interactions *or* events with only final state radiation (i.e. e^+e^- -like events) are both expected to have a current region hadronic state characteristic of a quark recoiling with energy $\sim Q/2$ and with only a z component of momentum. Boson-gluon fusion (BGF) events with a depleted, or empty, current hemisphere or events with significant initial state QCD radiation would, on the contrary, have a current region hadronic final state with significantly less energy at an angle to the z axis.

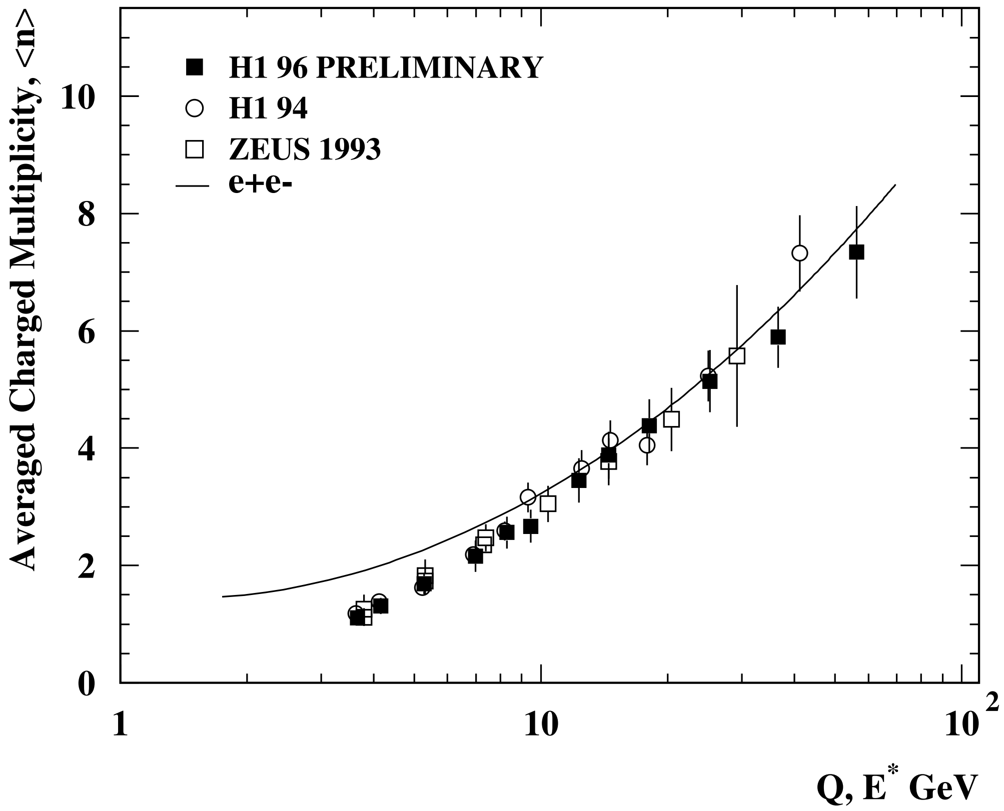

Figure 4: *Average charged multiplicity in the current hemisphere of the Breit frame as a function of Q for this analysis (solid circles) and for the ZEUS 1993 analysis (open squares). Statistical errors and systematic errors are added in quadrature. The curve is a fit to many e^+e^- results as a function of the centre of mass energy, E^*.*

7 Invariant Energy Spectra

At low momenta, or high values of ξ, fragmentation may be better studied using the event–normalised invariant spectrum, $(1/N) \times E\mathrm{d}n^{\pm}_{tracks}/\mathrm{d}^3p$. Perturbative QCD calculations [27] based on the MLLA and LPHD, predict that the hadronic spectrum at low momentum should be nearly independent of the energy of the parent parton. Here we follow [27] in taking $\mathrm{d}^3p = 4\pi p^2_{hadron}\mathrm{d}p_{hadron}$ and by computing the energy, E, of each track as if it had a mass of 270 MeV representing a presumed cut-off, $\sim \Lambda_{QCD}$, for the parton shower. The data are corrected for acceptance with the same bin-by-bin method described in section 3 with bin widths always greater than the resolution. The resulting purities for each data point shown are in the range 80% at low E to 40% at high E. For the reasons given in section 4, ep experiments can get closer to the critical low energy limit without serious loss of acceptance, than can e^+e^- experiments.

The results are shown in Fig. 5 binned into twelve intervals of photon virtuality, Q. The indicated errors contain contributions from statistical and all systematic effects discussed added in quadrature. The solid lines show MLLA/LPHD predictions at the relevant Q values for quark fragmentation using the calculations of [27]. The discrepancies get bigger at low Q and higher energies, E, and were shown in our previous paper [2] to be related to the same contributions from leading order, especially boson-gluon fusion, diagrams that give differences from e^+e^- data discussed in the previous section. Note that, as presented here, there is no attempt to apply any further data selections to reduce these differences. At the higher Q values the data show a clear tendency to approach a common limit at low particle energy, independent of Q and in agreement with the prediction.

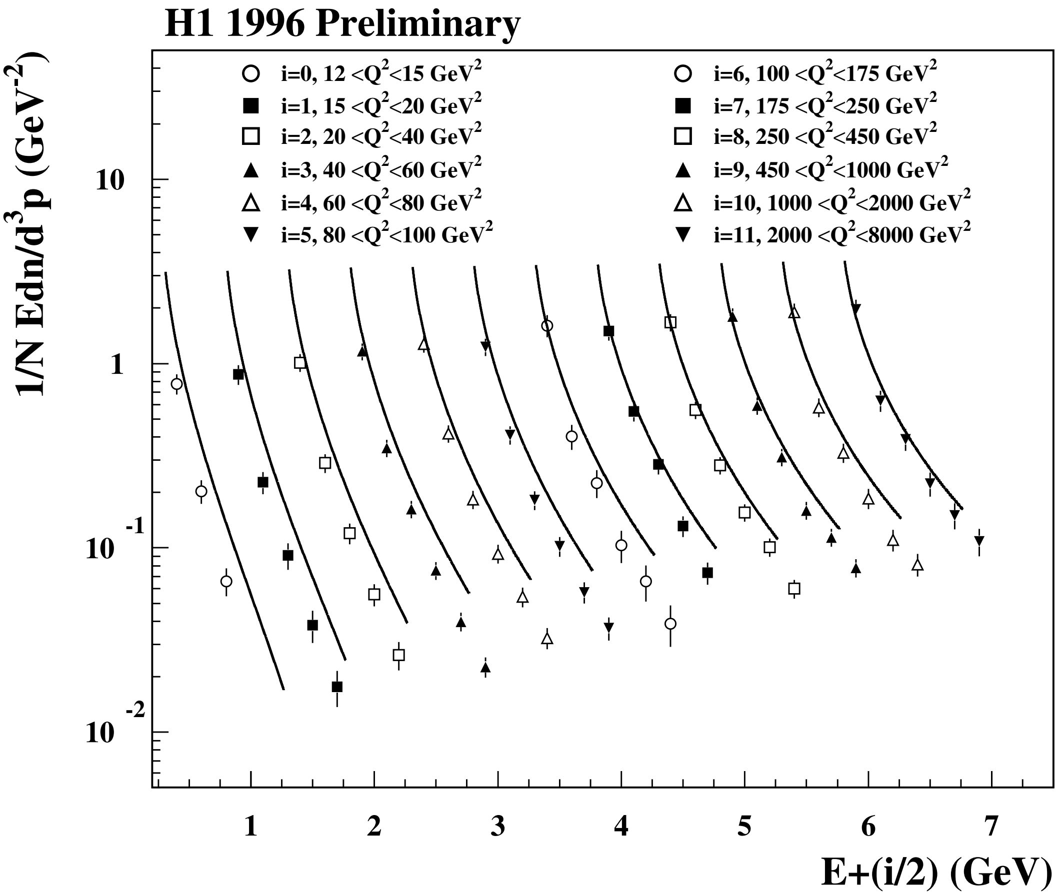

Figure 5: *The invariant charged hadron energy spectrum in the current hemisphere in twelve intervals of Q^2, with a regular incremental spacing of 0.5 GeV on the abscissa. The solid lines show the prediction of MLLA/LPHD calculated at the $\langle Q \rangle$ for each distribution. The error bars show the sum of statistical and systematic errors added in quadrature.*

8 Rapidity Spectra

The analyses thus far essentially use just the magnitude of charged particle momenta in the Breit Frame. Knowledge of the polar angle enables a study of the pseudo-rapidity, $\eta = -\ln\tan\theta_{Breit}/2$. The approximation of this variable to the rapidity, $Y = \frac{1}{2}\ln\left(\frac{E+p_z}{E-p_z}\right)$, is poor in the low transverse momentum region, where we would like to do measurements, so we continue the procedure of assuming a pion mass for every charged particle and use Monte Carlo simulations to correct for the non-pion contribution. Typical FWHM resolutions in the Breit Frame variables are $\Delta Y \sim 0.2$ and $\Delta p_t \sim 0.05$ GeV and bin purity levels are always above 35% and above 60% in the central region.

The resulting rapidity distributions for all charged particles may be seen in Fig. 6 and Fig. 7 for the low and high Q^2 data respectively, both integrated and divided into five intervals of p_t^{BREIT}, track transverse momentum. All figures are normalised by the total number of events (N) which pass the relevant cuts. The errors are a sum in quadrature of statistical and systematic effects from the sources already discussed. For the most part correction factors differ from unity by less than 20% but in attempting to carry the analysis as far into the forward (positive z, Y) direction as possible, this is relaxed in the most positive bins where acceptance falls to only 20%, and systematic errors increase accordingly.

The flat plateau, predicted by Bjorken [28] and Feynman [29] in the context of the simple parton model, is evident at low transverse momenta (p_t). The current (negative z, Y) hemisphere extends as $\ln Q$ in going from the low to the high Q^2 sample. Comparing Fig. 6 and Fig. 7, it is noticeable that the peak rapidity density hardly changes except above 1 GeV. As the p_t increases, QCD effects gradually evolve the flat plateau into an almost Gaussian structure peaking near zero, thus explicitly displaying the special role of the Breit Frame. Since the hadronic centre of mass is collinear with the Breit Frame, the origin of this frame is displaced by a constant amount dependent on $\langle Q \rangle$ of the sample and indicated on the figures by a small arrow.

In both figures the data is superimposed on the expectations from two leading order perturbative QCD Monte Carlo simulations employing respectively a color dipole model [12] and a DGLAP parton shower model [14] with JETSET [30] string hadronisation. Both of these models have some agreement with the H1 data but at low Q^2, as found earlier [31] the parton shower model predicts insufficient high p_t charged hadrons, especially in the forward region. An alternative form of the parton shower model which employs soft colour interactions predicts much too large multiplicities at intermediate p_t in the target hemisphere, and even more so at high Q^2.

Naïve expectations [32] are for a sharp rise followed by a plateau to be seen in the current hemisphere with a total width in Y proportional to $\ln Q$. Although the extension in Y with $\langle Q \rangle$ is clear, there is no separate plateau in this region. The dominance of QCD LO effects at low x, Q^2 destroys jet alignment, but the data is characterised by a slow and gradual fall off at *all* values of Q^2 and this extends well into positive Y at low p_t. For such particles, reflecting low p_t partons, predictions based on LPHD indicate the appearance of two distinct plateaux with a 9/4 ratio in their respective heights reflecting the colour charge of the dominant gluonic radiation in the target hemisphere [27, 33]. Despite many tests to isolate events in which such behaviour might be expected to be

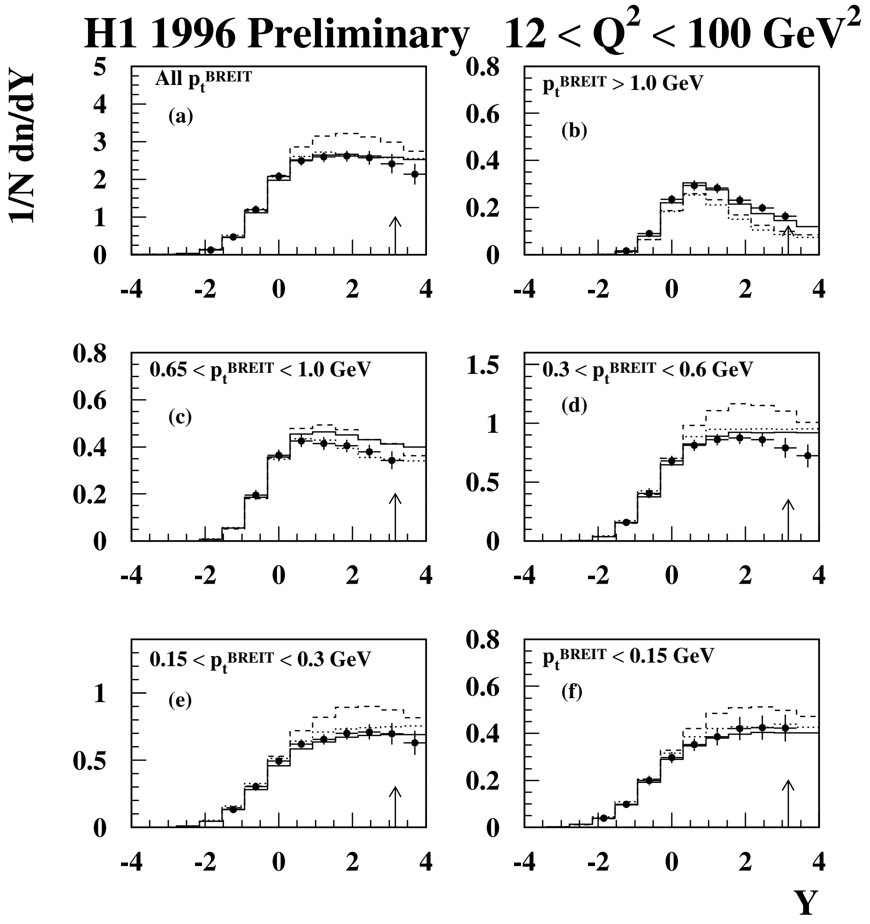

Figure 6: *The rapidity distribution for (a) all charged tracks, and (b-f) for the five indicated intervals of track transverse momentum,* p_t^{BREIT}*, in the Breit frame, all at low* Q^2*. The error bars show the sum of statistical and systematic errors added in quadrature. The arrow indicates the position of the origin of the hadronic centre of mass system for the* $\langle Q \rangle$ *(5.4 GeV) of the data. The histograms show the predictions of LO QCD Monte Carlo models, the solid line utilising a colour dipole fragmentation, the dashed(dotted) lines utilising a parton shower with(without) soft colour interaction effects.*

amplified, we have been unable to observe it.

9 Summary

A Breit frame fragmentation function analysis using the higher statistics of 1996 data confirms that NLO calculations give good predictions of the observed violations of fragmentation scaling. The differences between fragmentation in the e^+e^- and the ep final hadronic state are well measured and qualitatively understood in terms of leading order QCD effects which differ in the two cases. Rapidity plateaux have been studied and are

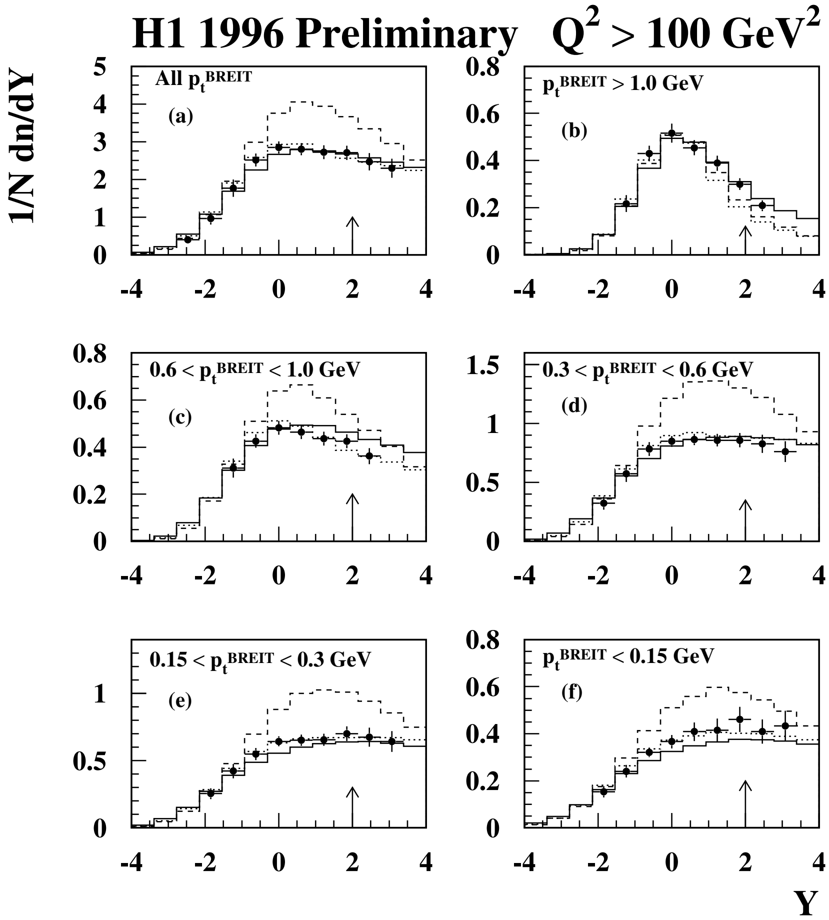

Figure 7: *The rapidity distribution for (a) all charged tracks, and (b-f) for the five indicated intervals of track transverse momentum, p_t^{BREIT}, in the Breit frame, all at high Q^2. The error bars show the sum of statistical and systematic errors added in quadrature. The arrow indicates the position of the origin of the hadronic centre of mass system for the $\langle Q \rangle$ (23 GeV) of the data. The histograms show the predictions of LO Monte Carlo models, the solid line utilising a color dipole fragmentation, the dashed(dotted) lines utilising a parton shower with(without) soft colour interaction effects.*

well described by a colour dipole model of QCD radiation. A parton shower model shows a deficiency of high transverse momentum tracks in the target hemisphere for events of low Q^2, whereas a version with soft colour interactions has a significant excess at low transverse momentum. The predicted step between the current and target regions of rapidity spectra remains unidentified.

Acknowledgments

We are grateful to the HERA machine group whose outstanding efforts have made and continue to make this experiment possible. We thank the engineers and technicians for their work in constructing and now maintaining the H1 detector, our funding agencies for financial support, the DESY technical staff for continual assistance, and the DESY directorate for the hospitality which they extend to the non–DESY members of the collaboration. We are grateful to D. Graudenz for kind assistance with obtaining NLO fragmentation predictions, to S. Lupia for assistance with generating MLLA predictions, and to W. Ochs for help and guidance with expectations for rapidity distributions.

References

[1] H1 Collaboration, S. Aid et al., *Nucl. Phys.* B **445**, 3 (1995).

[2] H1 Collaboration, C. Adloff et al., *Nucl. Phys.* B **504**, 3 (1997).

[3] ZEUS Collaboration, M. Derrick et al., *Z. Phys.* C **67**, 93 (1995) and contributed paper to 6th International Workshop on DIS and QCD , Brussels, April 1998.

[4] H.F. Jones, *Nuovo Cimento* **40**, 1018 (1965).

[5] K.H. Streng et al., *Z. Phys.* C **2**, 237 (1979).

[6] H1 Collaboration, I. Abt et al., DESY preprint 93-103 (1993), *Nucl. Instrum. Methods* A **386**, 310 (1997) (Vol 1) and *ibid.* p.348 (Vol 2).

[7] J. Bürger et al., *Nucl. Instrum. Methods* A **279**, 217 (1989).

[8] H1 FTD group, S. Burke et al., *Nucl. Instrum. Methods* A **373**, 227 (1996).

[9] H1 calorimeter group, B. Andrieu et al.,*Nucl. Instrum. Methods* A **336**, 460 (1993).

[10] H1 SPACAL group, R.D. Appuhn et al., DESY preprint 96-171 (1996), submitted to *Nucl. Instr. and Meth.*

[11] Proceedings of the study of an ep facility for Europe, Ed. U. Amaldi, DESY 79/48 (1979) p391-4.

[12] G.A. Schuler and H. Spiesberger, Proceedings of the Workshop: Physics at HERA, vol. 3 eds. W. Buchmüller, G. Ingelman, DESY (1992) 1419. We use version 6.2 with QED radiation simulated with HERACLES 4.4 when correcting data. QCD radiation is simulated by the colour dipole model (ARIADNE 4.08) and hadronisation with the LUND string model in JETSET 7.4. We use MRSH parton density parameterisations.

[13] R. Brun et al., GEANT3 User's guide, CERN-DD/EE 84-1, Geneva (1987).

[14] LEPTO 6.5 Generator with GRV parton density functions ; G. Ingelman, Proceedings of the Workshop: Physics at HERA, vol. 3 eds. W. Buchmüller, G. Ingelman, DESY (1991) 1366. We use versions with and without soft colour interactions (SCI).

[15] K.T. Donovan, *in litt.* University of London thesis; P. Dixon, University of Lancaster thesis (1997).

[16] H1 Collaboration, C. Adloff et al., *Nucl. Phys.* B **497**, 3 (1997).

[17] D. Graudenz, CERN TH/96-52, CERN TH/96-187 (hep-ph/9610287), CERN TH/96-155 (hep-ph/9606460), PSI-PR/97-20 and private communications.

[18] Yu.L. Dokshitzer, V.A. Khoze, A.H. Mueller and S.I. Troyan, "Basics of Perturbative QCD" Editions Frontières (1991); Ya.I. Azimov, Yu.L. Dokshitzer, V.A. Khoze, and S.I. Troyan, *Z. Phys.* C **31**, 213 (1986), *Z. Phys.* C **27**, 65 (1985); L.V. Gribov, Yu.L. Dokshitzer, V.A. Khoze, and S.I. Troyan, *Phys. Lett.* B **202**, 276 (1988).

[19] TASSO Collaboration, W. Braunschweig et al., *Z. Phys.* C **47**, 187 (1990).

[20] DELPHI Collaboration, P. Abreu et al., *Phys. Lett.* B **311**, 408 (1993); OPAL Collaboration, G. Alexander et al., *Z. Phys.* C **72**, 191 (1996).

[21] OPAL Collaboration, M.Z. Akrawy et al., *Phys. Lett.* B **247**, 617 (1990); ALEPH Collaboration, R. Barate et al., CERN PPE 96-186; DELPHI Collaboration, P. Abreu et al., *Z. Phys.* C **73**, 11 (1997).

[22] TOPAZ Collaboration, R. Itoh et al., *Phys. Lett.* B **345**, 335 (1995)

[23] DELPHI Collaboration, P. Abreu et al., *Z. Phys.* C **73**, 229 (1997); OPAL Collaboration, K. Ackerstaff et al., *Z. Phys.* C **75**, 193 (1997).

[24] OPAL Collaboration, P.D. Acton et al., *Z. Phys.* C **53**, 539 (1992).

[25] TASSO Collaboration, M. Althoff et al., *Z. Phys.* C **22**, 307 (1984).

[26] OPAL Collaboration, R. Akers et al., *Z. Phys.* C **61**, 209 (1994).

[27] V.A. Khoze, S. Lupia, and W. Ochs, *Phys. Lett.* B **394**, 179 (1997) and hep-ph/9711392 (to be published in *Eur. Phys. J.* C), and V.A. Khoze, hep-ph/9712396.

[28] J.D. Bjorken and E.A. Paschos, *Phys. Rev.* **185**, 1975 (1969).

[29] R.P. Feynman and R.D. Field, *Nucl. Phys.* B **136**, 1 (1978).

[30] T. Sjöstrand, *Computer Phys. Comm.* **39**, 346 (1986); T. Sjöstrand, M. Bengtsson, *Computer Phys. Comm.* **43**, 367 (1987).

[31] H1 Collaboration, C. Adloff et al., NPB **485**, 3 (1997).

[32] R.N. Cahn, J.W. Cleymans and E.W. Colglazier, PLB **43**, 323 (1973).

[33] W. Ochs, Proc. of the Ringberg workshop "New Trends in HERA Physics", Tegernsee, Germany, 25-30 May 1997. hep-ph/9709248.